

# Electronic properties of DNA: structural and chemical influence on charge transfer and the quest for high conductance

R.G. Endres, D.L. Cox, R.R.P. Singh

*Department of Physics, University of California, Davis, CA 95616*

(Dated: December 2, 2024)

## Abstract

Motivated by the wide ranging experimental results on the conductivity of DNA, we investigate extraordinary configurations and chemical environments in which DNA might become a true molecular wire. In particular, we examine A- vs B-DNA, the ribbon-like structures proposed to arise from molecular stretching, the potential role of counterions in hole doping the DNA orbitals, and the possibility of backbone conduction. We further discuss the role of harmonic vibration and twisting motion on electron tight binding matrix elements using *ab initio* density functional theory and model Koster-Slater/Hückel theory calculations. We find that partial cancellation between  $pp\sigma$  and  $pp\pi$  interaction of  $p_z$  orbitals on adjacent base pairs, along with destructive interference of phase factors are needed to explain the weak conductance of A DNA and angular dependence of inter-base pair tight binding matrix elements. Furthermore, we estimate Franck-Condon factors, reorganization energies and nuclear frequencies essential for charge transfer rates, and find our estimated hole transfer rates between base pairs to be in excellent agreement with recent picosecond dynamics data.

PACS numbers:

## I. INTRODUCTION

In addition to DNA's fundamental role in genetics, it is now also a potential candidate for nano-electronic devices. The highly specific binding between single strands of DNA and its self-assembly property open a whole new approach to single-molecule electronics. However, its intrinsic conductance properties remain highly controversial. As early as 1962, Eley and Spivey suggested that  $\pi - \pi$  interactions of stacked base pairs in double stranded DNA could lead to conducting behavior[1]. Recently, there have been several experimental studies of the DNA conductance, leading to a variety of results. These have ranged from wide-gap insulating behavior to proximity induced superconductivity.

Although double stranded DNA has similarities to van der Waals stacked aromatic conducting crystals (*e.g.* the DNA base pair spacing is similar to the preferred axis lattice spacing of aromatic crystals) it also has essential differences from these and conventional conductors. Unlike crystals, the DNA is not a periodic system. The largest ionization potential difference between two isolated bases is about 0.6 eV between guanine and thymine which exceeds the electronic coupling between base pairs. Thus, the base pair sequence plus DNA's environment, like water and counterions, can have a substantial impact on its conductivity. From molecular dynamics simulations, the average displacement of a base pair in DNA is about  $0.4\text{\AA}$  [2] which is a tenth of the lattice constant and an order of magnitude higher than in crystals at RT. All these properties make DNA a highly dynamic system and it remains unclear how well traditional concepts from solid state physics can describe it.

DNA has recently been the object of numerous single molecule studies to ascertain its conducting properties directly. Results have varied dramatically, from finding a fully localized insulator[3], a wide gap semiconductor with coherent extended states[4], a metal at room temperature with ohmic current voltage characteristics and a conductance comparable to doped polyacetylene[5], and, most shockingly, a proximity effect superconductor at very low temperatures[6]. Recently, self-assembled networks of DNA have been developed with quite reasonable conductance properties over distance scales of 50 nm or less, and high conductance induced by chemical or gated doping[7]; these networks can be used to make transistor devices.

Motivated by these wide ranging experimental results on the conductivity of DNA, we have embarked on a theoretical effort to ascertain what conditions might induce such re-

markable behavior. In particular (sec. II), we have studied the influence of structure (a hypothetical stretched ribbon structure, A, and B form DNA have been examined) and counterions (especially sodium and magnesium). We have used a combination of fully ab initio density functional theory code (SIESTA[8]), and a parameterized Hückel-Slater-Koster modelling using only atomic  $p_z$  orbitals ( $z$  the long axis of the molecule) of the bases. We have been unsuccessful in identifying structural motifs that might engender metallic conductance in DNA. We do find that Mg counterions allowed to condense in the major grooves of poly(G)-poly(C) DNA tend to donate a hole which leads to donor state formation just above the HOMO and potential enhanced conduction. We find that while direct HOMO-HOMO or LUMO-LUMO matrix elements for model DNA are small (order 0.1 eV), individual matrix elements between  $p_z$  orbitals on well contacted atoms in adjacent base pairs can exceed 1 eV.

We have also studied the influence of longitudinal and torsional vibrations upon the electronic structure of DNA (sec. III), and estimated reorganization energies, Franck-Condon factors, and charge transfer rates between adjacent bases (sec.IV). We find good agreement between our estimated rates and recent experimental data[9] assuming that torsional (twist) vibrations limit the charge transfer most significantly.

## II. THEORETICAL SEARCH FOR HIGH CONDUCTANCE DNA

### A. Structural influence

In this section we demonstrate that the electronic coupling between base pairs is highly sensitive to the DNA structure and thus to the influence of its environment, which can modify the structure.

In biological situations, there are several double helical conformations of DNA depending on the humidity and salt concentration. We consider the A and B forms, . The B form predominantly occurs *in vivo*, has a unit cell of 10 base pairs (neglecting sequence effects), a helical rise of about  $3.375\text{\AA}$  per base pair, and a twist angle between adjacent base pairs on average of  $36.0^\circ$  [10]. Since the base pairs are approximately perpendicular to the helical axis, the base pair separation is close to the helical rise . The A form exists at low humidity. The double helix is relaxed to 11 base pairs in a unit cell exposing more of the hydrophobic

core of base pairs and portions of the sugar units of the back bone. The helical rise and base pair separation are  $2.56\text{\AA}$  and  $2.425\text{\AA}$ , respectively. The twist angle is only  $32.7^\circ$ [11].

There are also other known conformations. In order to obtain straight DNA molecules for conductivity measurements, one often uses a technique called molecular combing [12]. When a DNA molecule is anchored at one end on a hydrophobic surface like polystyrene, a receding meniscus can stretch DNA by a factor of 1.7, or if grafted at both ends to the surface even by a factor as large as 2.1. The capillary forces are typically  $> 160pN$  and can become as large as  $500pN$  which results in breaking the molecule. The stretching has been theoretically examined with molecular dynamics simulations using classical force fields [13]. Since the phosphate-phosphate distance along the backbone is about  $7\text{\AA}$  and the base pair separation in B DNA is about  $3.4\text{\AA}$ , stretching by a factor of 2 can, in principle, lead to a complete unwinding of the double helix. Since just stretching would weaken the inter base pair electronic coupling, we examine the possibility of base pairs lying in the plane of the backbone strands (fig.1). In this case, the base pairs can come close again and the kinetic energy of the  $\pi$  electrons can in principle be lowered if there was decent  $pp\pi$  overlap between the  $p_z$  atomic orbitals at the closest contacts (with the z-axis now perpendicular to the ribbon). Ribbon-like structures are indeed found by K.M.Kosikov *et al* [13], e.g. the structures  $A_1$  or  $B_1$ , by using the the AMBER force field.

In order to get a realistic picture of the electronic coupling strength between two base pairs, the smallest structural unit through which charge has to go, we use the DFT code SIESTA [8]. Since its aim is efficiency and large systems, it uses (norm-conserving) pseudo potentials, and a basis set of (numerical) atomic orbitals. We used a double- $\zeta$  basis set with polarization orbitals (DZP), the largest basis within SIESTA, and the generalized gradient approximation for the exchange-correlation energy functional. The structures for A and B DNA were obtained from x-ray diffraction data [11] and [10], respectively. Since the hydrogen atoms were missing in the A DNA structural data, they were added and relaxed with the conjugate gradient method. The ideal 2-dimensional ribbon structure of figure 1 was created artificially in order to get most effective  $pp\pi$  overlap and a small unit cell containing only a single base pair. As for the 2 base pair calculations, only methylated base pairs without the backbone were used for simplicity. The electronic coupling between the HOMO and LUMO molecular orbitals of a single base pair are shown in table I. The numerical values were obtained using formulas for non-orthogonal states[14], *viz*

$$t_{12} = [t'_{12} - 0.5(t'_{11} + t'_{22})S_{12}](1 - S_{12}^2)^{-1} \quad (1)$$

$$t'_{12} = \sum_{i,j} c_i^1 c_j^2 H_{ij}, \quad S_{12} = \sum_{i,j} c_i^1 c_j^2 S_{ij}, \quad (2)$$

where  $c_i^n$  is the  $i$ th LCAO coefficient of a specific molecular orbital of the  $n$ th base pair, and  $H_{ij}$ ,  $S_{ij}$  are the Hamiltonian and overlap matrices of the two base pair system. The values for the B form are, in general, small and in good agreement with earlier *ab initio* studies [15], but for A and ribbon form they are even smaller than for the B form. For the ribbon structure, we also did a band structure calculation with 10 k points including backbone and full relaxation. There was no sign of dispersion in agreement with the weak electronic coupling.

Thus, our conclusion is that dehydrating (A conformation) and stretching of DNA should lead to even more highly localized states and insulating behavior than in B-DNA. For the ribbon, the main reason is that there are only very few close contacts between neighboring base pairs (see also figure 1). For A DNA, the weak coupling might seem a bit surprising since the base pair separation is much smaller than in B DNA, but it can be understood in terms of less effective stacking, i.e., there are fewer direct contacts between  $p_z$  orbitals pointing at each other. Another important reason is that there are  $pp\sigma$  and  $pp\pi$  interaction between  $p_z$  orbitals (fig. 2) which have opposite signs, which partially cancel each other.

In order to understand this result more quantitatively, we assume a Slater-Koster form for the two types of interactions [16]

$$V_{pp\sigma} = \eta_{pp\sigma} \frac{\hbar^2}{md_o^2} e^{-d/R_c} > 0 \quad (3)$$

$$V_{pp\pi} = \eta_{pp\pi} \frac{\hbar^2}{md_o^2} e^{-d/R_c} < 0, \quad (4)$$

where  $d$  and  $m$  are distance and electron mass, and  $(\hbar^2)/(md_o^2) = 7.62eV$ . The exponential distance cut-off  $R_c$  and  $\eta$  are parameter to be determined by fitting. The interatomic matrix element between two ‘‘parallel’’  $p_z$  orbitals is then

$$\begin{aligned} E_{zz} &= \sin^2 \phi V_{pp\sigma} + \cos^2 \phi V_{pp\pi} \\ &= \frac{\hbar^2 e^{-d/R_c}}{md_o^2} \left[ (\eta_{pp\sigma} + |\eta_{pp\pi}|) \frac{z^2}{l^2 + z^2} - |\eta_{pp\pi}| \right], \end{aligned} \quad (5)$$

which shows the interplay between the two interactions. The local  $z$  axis can be defined by the normal of the corresponding base. A general formula for non-parallel orbitals, which is used for all our model calculations can be found in the Appendix, eq. (A3). The combination of close base pair separation *and* poor contacts reduces the electronic coupling between base pairs. As a further illustration, figure 3 shows a distribution of all possible  $p_z$  interatomic matrix elements between two  $G \cdot C$  base pairs. Since guanine and cytosine have 11 and 8  $p_z$  orbitals, there is a total of  $19 \times 19 = 361$  matrix elements. (Adenine and thymine have 10 and 8  $p_z$  orbitals respectively.) It is important to keep in mind that the graph is only a sampling over all matrix elements between individual atomic-like  $p_z$  orbitals on adjoining base pairs, and it does not say anything about the HOMO or LUMO states. What it shows is that there are more good contacts, e.g. above 0.75 eV twice as many, in the B form. Furthermore, there is a shift to (negative)  $pp\pi$  interaction in the A form, although a single optimal contact is leading to a quite large interaction matrix element due to the shorter distance. The plots were obtained using the x-ray structures for A and B DNA, where a plane was first fitted to each single base whose normal is taken for the direction for all  $p_z$  orbitals within that base.

The Slater-Koster parameters  $\eta_{pp\sigma}$ ,  $\eta_{pp\pi}$  and cut-off  $R_c$  were determined from fitting to DFT data as follows: Starting from the DZP basis of SIESTA, we first identify the orbitals of  $p_z$  symmetry which compare most directly to the Hückel orbitals. These are the first- $\zeta$  orbitals of  $p_z$  symmetry. We consider the reduced SIESTA Hamiltonian matrix in this basis, which has two diagonal blocks representing the on-site and intra-base pair couplings and one off-diagonal block representing inter-base pair couplings. The Slater-Koster matrix elements calculated with eq. (A3) are directly fitted to the off-diagonal block matrix elements. The fitting was done with simulated annealing, which gave better (and still physical) results than e.g. with the Powell algorithm. However, since the DFT code uses a global  $z$ -axis along the helix which is different from the local  $z$ -axis due to an inclination and a propeller twist angle associated with each base, we turn to parallel reference base pairs for the fitting process. In case of A DNA we use two parallel  $G \cdot C$  base pairs with a separation of  $2.425\text{\AA}$ , while for B DNA ones with a separation of  $3.375\text{\AA}$ . The fitted parameters are  $\eta_{pp\sigma} = 2.9309$ ,  $\eta_{pp\pi} = -0.7254$ ,  $R_c = 1.1552\text{\AA}$  for A DNA, and  $\eta_{pp\sigma} = 5.2704$ ,  $\eta_{pp\pi} = -2.2571$ ,  $R_c = 0.8741\text{\AA}$  for B DNA. Since A DNA appears electronically uninteresting[3], we restrict ourselves to B DNA in the subsequent discussion.

What is potentially useful about the result that large transfer matrix elements exist between individual atomic orbitals is that it opens the door to a mechanism for enhanced interbase conduction at least at rapid, non-equilibrium time scales for electrons/holes injected into DNA. Namely, if strong coupling to intra-base vibrations limits the formation of coherent molecular orbital states on a given base pair, it may be possible for the electron/hole to delocalize along the DNA first rather than in the base pair. It will be interesting to explore whether any experimental conditions can lead to this possibility.

## B. Counterions

DNA is a highly charged molecule which can only be stable if the negatively charged phosphate groups are neutralized by positive counterions from a buffer solution. In order to measure its conductivity DNA has initially to be dried. The counterions are assumed to condense in the grooves and so stay with the DNA molecule. Different research groups in general work with different buffer solutions: semi-conducting behavior with an initial sodium ion buffer was observed by Kawai's group *et al* [7] using poly(G)-poly(C)/poly(A)-poly(T) DNA self-assembled networks, DNA networks, and by Porath *et al* [4] who used single 10.4-nm-long poly(G)-poly(C) DNA molecule. On the other hand, proximity effect superconductivity was observed by Kasumov *et al* [6], who used a few 16- $\mu\text{m}$ -long  $\lambda$ -DNA molecules taken from a magnesium buffer solution.

Motivated by this, we have examined the effects of various counterions (protons, Na, Mg) on the electronic structure of B-DNA. We take 4 base pair long poly(G)·poly(C) B DNA with each strand containing 5 phosphate groups, and also include a proper amount of counterions to make the overall system charge neutral. The proton counterions are placed at the phosphates where they bind covalently, while the sodium and magnesium are placed partially in the grooves and along the backbone [17] where they stay ionic. We do not optimize the geometry with the conjugate gradient method, but place the metal ions at different locations to make sure no drastic changes occur in the band structure or Mulliken population of the ions. Besides, at finite temperature, the ions can be expected to be moving around due their weak binding. We use a double- $\zeta$  basis set except for phosphorus, for hydrogens involved in hydrogen bonding and the counterions for which we also include polarization orbitals. The density of states (PDOS) is then projected onto atomic orbitals

for energies around the Fermi energy  $\epsilon_F$  to see which atomic orbitals can contribute to charge transport and what effects the counterions have on the eigenvalue spectrum.

The PDOS of the  $i$ th atomic basis orbital projected on the  $n$ th molecular orbital is

$$\rho_i^n(\epsilon) = \sum_j^{N_B} c_i^n c_j^n S_{ij} \delta(\epsilon - \epsilon_n), \quad (6)$$

where  $N_B$  is the dimension of the basis set,  $c_i^n, c_j^n$  are the LCAO coefficients and  $S_{ij}$  are the atomic overlap matrix elements. Figure 4 shows the PDOS of the  $p_z$  orbitals of elements C, N and O within a base pair ( $\pi$  and  $\pi^*$  molecular orbitals), all orbitals of phosphate atoms P,O3 and O5 (conventional notation), all orbitals of the following sugar atoms C3,4,5 and H3,4,15,25, as well as counterions. The phosphate (green) and sugar (blue) atoms are chosen in such a way that a hypothetical charge transport through the back bone would have to involve these atoms.

In the case of proton counterions (yellow), one obtains the expected  $\pi$  and  $\pi^*$  molecular orbital picture, while for the metal ions (yellow) the effect on the gap and atomic character of states around the  $\epsilon_F$  are quite drastic. The gap disappears, and only a finite level spacing remains. The occupied phosphate states gain in energy relative to  $\pi$  orbitals. In the case of sodium, for example, they fill the  $\pi$  and  $\pi^*$  gap, resulting in phosphate states around the Fermi energy, as well as low lying metal states and  $\pi^*$  orbitals above  $\epsilon_F$ .

For magnesium, the result is even more interesting and is shown in more detail in figure 5. There is an even higher DOS at  $\epsilon_F$  with an additional stronger admixture of  $\pi$ , phosphate and magnesium states. This is due to doping effects by magnesium ions. The Mulliken population of all the counterions which shows the following electronic charges for hydrogen, sodium and magnesium:  $1.1 e^-$  (covalent H),  $0.1-0.2 e^-$  (ionic  $\text{Na}^+$ ) and  $1.1 e^-$  (ionic  $\text{Mg}^+$ ). Within our pseudo-potential code calculation, magnesium seems to be monovalent leading to hole doping relative to fully negatively charged DNA.

This raises the question: can magnesium counterions can make DNA conducting as found by Kasumov *et al* [6]? Looking at figure 5, one can hypothesize that electrons could be (thermally) excited from the occupied phosphate (green) or even lower  $\pi$  orbitals (red) to the empty atomic s-type magnesium states (yellow) right above  $\epsilon_F$  which could lead to hole transport through the back bone and to a lesser extent through the base pairs. Another possibility is electron transport through magnesium impurity states.



The problem with hole transport through the back bone is that the sugars (blue) - which separate the phosphates - contribute very little to the relevant molecular orbitals, while electron transport mediated by magnesium suffers from well separated magnesium orbitals. This is supported by charge density plots of HOMO and LUMO states which show well localized phosphate and atomic like metal states not well suited for effective charge transport.

### III. DYNAMICAL INFLUENCE ON ELECTRONIC STRUCTURE

At finite temperature the base pairs of DNA will be oscillating about their equilibrium positions. Within our model from section II A we are ultimately interested in the average electronic coupling between two base pairs at temperature  $T$ . For this purpose it is assumed that displacements along and twisting motion about the helix axis are the most important degrees of freedom. For small changes in the variables, one can assume that these two degrees of freedom are independent.

Let  $\phi$  and  $u$  describe the deviations from equilibrium twist angle and base pair separation. Within our Hückel-model, the transfer integral between two molecular orbitals of adjacent base pairs is determined in the CNDO approximation by  $t = \sum_{i,j} V_{ij}c_i c_j$  where the LCAO coefficients are summed over each of the two base pairs and kept fixed for all  $\phi$  and  $u$ , and are given by the first- $\zeta$  orbitals of  $p_z$  symmetry from a single base pair DZP calculation. These are corrected by a factor  $\cos^{-1} \theta$  where  $\theta = 8.0^\circ$  is the angle between the local base normal and the helical axis. Since we always calculate only transfer integrals with CNDO, we do not need on site energies here. Nevertheless, these can be easily obtained in the same fashion. The resulting model can be used for very large scale quasi-self-consistent-field quantum calculations of long DNA sequences - similar to the one used for electron transfer rate calculations between various donors and acceptors in DNA[18].

In figures 6 and 7 one can see the electronic coupling between the frontier orbitals as a function of one of the variables  $\phi$  or  $u$ . The other one is kept fixed at the equilibrium value. At  $\phi = -36^\circ$  the coupling is maximal and positive. If we assume for simplicity a GG dimer, then this is caused by 19 optimal contacts, and the transfer integral is approximately given by  $t \sim \sum_i V_{ii}c_i^2$  where  $V_{ii} > 0$  due to solely  $pp\sigma$  interaction. More interesting is the fact that there are sign changes of  $t(\phi)$  in figure 6 leading to local maxima earlier observed

in *ab initio* studies [15]. In B DNA, all the interaction matrix elements are essentially positive ( $pp\sigma$  dominated), as can be seen in figure 3 and this is true for arbitrary twist angles  $\phi$ . Since for larger twist angles, i.e.  $\phi \approx 0$ , the transfer integral is approximately given by  $t \sim \sum_{i \neq j} V_{ij} c_i c_j$ , the sign change of  $t$  can only come from the signs of the LCAO coefficients (phases of the  $p_z$  orbitals). This can lead to positive or negative  $t$ , or to a complete cancellation.

Coming back to the temperature dependence of  $t$ , we assume classical harmonic potentials with spring constant  $K$  and shear constant  $S$  for each couple of base pairs. They can be estimated using the equi-partition theorem from classical statistical mechanics and estimates for the standard deviation from molecular dynamics [13]

$$0.375^2 \text{\AA}^2 = \langle u^2 \rangle = \frac{k_B T}{K} \quad (7)$$

$$\longrightarrow K = 0.184 \frac{eV}{\text{\AA}^2} = 294.8 \frac{pN}{\text{\AA}} \quad (8)$$

$$7.5^2 \text{deg}^2 = \langle \phi^2 \rangle = \frac{k_B T}{S} \quad (9)$$

$$\longrightarrow S = 4.6 \cdot 10^{-4} \frac{eV}{\text{deg}^2}. \quad (10)$$

With these estimates for  $K$  and  $S$  the average electronic coupling can be calculated

$$\langle t \rangle_T = \frac{\int du d\phi t(u, \phi) e^{-\frac{\beta}{2}(Ku^2 + S\phi^2)}}{\int du d\phi e^{-\frac{\beta}{2}(Ku^2 + S\phi^2)}}, \quad (11)$$

with  $\beta = 1/k_B T$ . The transfer integral only depends on the differences  $u = u_2 - u_1$  and  $\phi = \phi_2 - \phi_1$ , where  $u_i$  and  $\phi_i$  are the displacement and twist angle of the  $i$ th base pair. The results are shown in figures 8 and 9. Two things are remarkable about this result. First, the temperature dependence is very weak (a few meV change over hundreds of K). Second, harmonic displacement along the helical axis alone can lead to an increase in magnitude of the electronic coupling with increasing temperature  $T$ , while twisting motion on the other hand has the opposite effect leading to a cancellation.

This can be understood by looking at figures 6 and 7. Since  $t(\phi = 0)$  is closer to a local maximum (at least for HOMO states), a broadening of the gaussian distribution  $\sim e^{-\beta S \phi^2 / 2}$  with increasing temperature about  $\phi = 0$  will give more contribution from smaller  $t$ . On the other hand, a broadening of the gaussian distribution  $\sim e^{-\beta K u^2 / 2}$  will

lead to more contributions from  $t$  with larger magnitude, since  $t(u)$  increases exponentially in magnitude when lowering  $u$ . These results are in contrast to Porath *et al* measurements of the temperature dependence of the voltage gap in the I-V curves[4]. The extremely strong increase of the gap (and hence strong decrease of the inter base pair hopping  $t$ ) with temperature could also be due to other effects, e.g. the contacts with the electrodes. The smallness of  $t$  does not allow much decrease anyway.

The physical significance of our calculation of eq. (11) is that since conductance is measured on a macroscopic time scale, the average transfer integral is the right one to consider, i.e. it is approximately constant with temperature.

#### IV. ESTIMATION OF PARAMETERS FOR CHARGE TRANSFER

Single electron or hole transfer, on the other hand, is likely to be very sensitive to the actual motion of base pairs. According to figure 6, the magnitude of the transfer integral oscillates between approximately 0 and 0.1-0.2 eV when one assumes a standard deviation of the twist angle of about  $10^\circ$  (actually more like  $7.5^\circ$ ). Under this assumption electron tunneling is possible on a time scale of the oscillation time  $T_S$  which can be estimated with  $T_S = 2\pi\sqrt{I/S}$ , where  $S$  is the shear constant and  $I = I_1 I_2 (I_1 + I_2)^{-1}$  the reduced moment of inertia of two base pairs.

More specifically, single charge transfer rates between two base pairs can be estimated from the classical Marcus formula [19] (neglecting nuclear tunneling effects)

$$k_{CT} = \nu_n \kappa_{el} e^{-\beta\Delta E^*}, \quad (12)$$

where  $\nu_n$  and  $\Delta E^* = (E_\lambda + E_o)^2/(4E_\lambda)$  are the nuclear frequency and energy to reach the transition state, while  $\kappa_{el}$  describes the electronic transmission coefficient.  $E_\lambda$  is the total reorganization energy and  $E_o \leq 0$  is the reaction energy which is zero for charge transfer between homogeneous base pairs.

First we note that we expect the charge transfer to be adiabatic, i.e.  $\kappa_{el} \approx 1$ , since the probability  $P = 1 - \exp(-2\pi\gamma)$  with

$$\gamma = \frac{t^2}{8\hbar\nu_n\sqrt{\pi k_B T \Delta E^*}} \quad (13)$$

for crossing the surfaces at the transition state [20] is close to unity. This is mainly due to the relatively large transfer integral  $t$ . Inner reorganization energies and nuclear frequencies associated with adjusting the bonds between atoms of a single base pair can be calculated as described in [21]. The results are shown in table II, which also contains estimates for moments of inertia. The resulting frequencies are quite similar to in-plane  $E_{2g}$  frequencies ( $4.8 \cdot 10^{13} 1/s$ ) in graphite [22], and our calculated inner reorganization energies lie between the ones of benzene (0.26 eV) and anthracene (0.07 eV) [21] as one would expect. Since the total reorganization energy is estimated to be only about 0.4 eV [23] which is close to our values for the inner reorganization energies from table III, we confirm that the base pairs must be well protected by the double helix formation and solvation effects can be neglected for now. The small reorganization energies also contribute to the adiabaticity according to eq. 13. An upper and lower bound for the charge transfer rates between two base pairs can be found in table III. For the upper bound,  $\nu$  in equation (12) is given by the high inner base pair nuclear frequencies, while a lower bound can be given by assuming that the low frequency twisting mode of base pairs is the time limiting step as described above. This process can be viewed as reaching some kind of encounter complex with a frequency  $\nu = 1/T_S$ . Interesting is the large Franck-Condon factor in table III for hole transfer in sequence AG. This is due to being close to the so called optimal electron transfer regime in which the reorganization energy (0.26 eV) is largely compensated by the reaction energy ( $0.20 \pm 0.05$  eV)[24].

Note that this reaction energy is smaller than the difference of the bare oxidation potentials (0.4–0.5 eV) between isolated adenine and guanine in a polar solvent [25]. Furthermore, hole transfer is in most cases at least one order of magnitude faster and hence more efficient.

In order to compare with experiment we turn to the (hole) transfer between initially excited 2-aminopurine (an isomer of adenine) and guanine [9]. The measured charge injection time of 10ps (corresponding to a rate of  $10^{11} 1/s$ ) is surprisingly close to our lower bound value  $4.1 \cdot 10^{11} 1/s$ . Hence we speculate that the twisting motion of base pairs is rate limiting.

Another simple application of the 2 base pair charge transfer rates of table III is the hole hopping between homogeneous sequences, e.g.  $(A \cdot T)_N$ , when one assumes (biased) random walk as the underlying mechanism of the charge migration. In this case, the rate shows a weak algebraic distance dependence[26]  $k_{CT} \approx k_{HOP} N^{-\eta}$ , where  $N$  is the number of intervening base pairs and  $1 \leq \eta \leq 2$ . Absolute rates can be predicted with our (lower

bound) value  $k_{\text{HOP}} = 9.88 \cdot 10^{10} 1/s \approx 10^{11} 1/s$ . In order to compare with experiment [27] one would have to include the initial transfer from the donor to the bridge, as well as the final transfer from the bridge to the acceptor which leads to a further reduction of the rate.

Finally, since charge transfer between adjacent base pairs is likely to be adiabatic, i.e. distance independent, one should avoid including these when fitting to a diabatic charge transfer rate  $k_{CT} \sim \exp(-\beta R)$ . Including these leads to an underestimation of the  $\beta$ .

## V. CONCLUSIONS

In summary, we have studied the electronic properties of DNA from several perspectives. Our initial motivation was to come up with possible conditions which enhance the conductance of DNA. For example, we expected a stretched ribbon-like DNA to be a potential candidate for a molecular wire. Unfortunately, that has not turned out to be the case. Indeed, in the ribbon-like DNA, the base pair separation can become quite small. However, the  $pp\pi$  interaction appears not very effective as there are only very few good contacts. Using the *ab initio* code SIESTA we compared transfer integrals between base pairs of A, B and stretched DNA. Our calculations suggest that dry DNA (A form) and stretched, ribbon-like DNA should support electrical current even less than B DNA.

More promising are doping effects by counterions. We showed with band structure calculations and the projected density of states method that counterions have strong effects on the molecular orbitals, i.e. the atomic species character of states and the size of the HOMO - LUMO gap. Especially magnesium could have a positive effect on the conductance. However, while the gap vanishes due to hole doping, the resulting states still appear to be localized and don't seem to support current easily - at least not as in conventional band conductors.

In order to get a better microscopic understanding of the electronic coupling and how it is affected by twisting and displacement of base pairs we developed a Hückel-Slater-Koster type model with parameters obtained from *ab initio* calculations. We find that the transfer integral is constrained by a competition between  $pp\sigma$  and  $pp\pi$  interaction and interference by phase factors of atomic  $p_z$  orbitals. The latter effect leads also to sign changes in the transfer integrals not observed previously.

Furthermore, the temperature dependence of the time averaged transfer integral is expected to be weak, first, because the electronic coupling is already weak anyway, and cannot be reduced much. Second, because twisting and displacement motion of base pairs have opposite effects which tend to cancel each other.

Next, we showed that charge transfer rates between adjacent base pairs are likely in the adiabatic limit. Thus, it is important to exclude these when obtaining  $\beta$  from fitting to a diabatic, exponentially decaying rate.

We also calculated Franck-Condon factors, reorganization energies and nuclear frequencies to obtain absolute rate estimates. Furthermore, we suggest that the twisting motion is very significant for charge transfer in the sense that it might be rate limiting. Due to the adiabaticity of the two base pair rates, DNA might be a good medium for diffusive charge transport.

*Acknowledgements.* We would like to thank P.Ordejón, E.Artacho, D.Sánchez-Portal and J.M.Soler for providing us with their *ab initio* code SIESTA. We acknowledge helpful conversations with J.K. Barton, C.Y. Fong, and J. Jortner. This work was supported by the U.S. Department of Energy, Office of Basic Energy Sciences, Division of Materials Research, by a faculty seed grant from the U.C. Davis office of research, by a collaborative seed grant from the Materials Research Institute of Lawrence Livermore National Laboratories, and by the National Science Foundation grant DMR-9986948.

## APPENDIX A: APPENDIX

In the following we derive a general formula for the calculation of interaction matrix elements between two atomic  $p_z$  orbitals belonging to adjacent base pairs. In general, the orbitals point in different directions, since the local z-axis is different for each base mainly due to a propeller twist angle, in case of A DNA also because of a large inclination angle. We first expand the orbitals  $p_z, p'_z$  in a global coordinate system with the z-axis pointing in the direction of the helix

$$\begin{aligned} p_z &= \alpha \tilde{p}_x + \beta \tilde{p}_y + \gamma \tilde{p}_z \\ p'_z &= \alpha' \tilde{p}_x + \beta' \tilde{p}_y + \gamma' \tilde{p}_z, \end{aligned} \tag{A1}$$

where the expansion coefficients are the direction cosines. If  $(l, m, n)$  is unit vector pointing from one orbital to the other, the Slater-Koster relations [16]

$$\begin{aligned}
E_{xx} &= l^2 V_{pp\sigma} + (1 - l^2) V_{pp\pi} \\
E_{yy} &= m^2 V_{pp\sigma} + (1 - m^2) V_{pp\pi} \\
E_{zz} &= n^2 V_{pp\sigma} + (1 - n^2) V_{pp\pi} \\
E_{xy} &= lm(V_{pp\sigma} - V_{pp\pi}) \\
E_{xz} &= ln(V_{pp\sigma} - V_{pp\pi}) \\
E_{yz} &= mn(V_{pp\sigma} - V_{pp\pi})
\end{aligned} \tag{A2}$$

can be used to obtain the following formula for the interaction matrix element

$$\begin{aligned}
V &= \alpha\alpha' E_{xx} + \beta\beta' E_{yy} + \gamma\gamma' E_{zz} \\
&\quad + (\alpha\beta' + \beta\alpha') E_{xy} + (\alpha\gamma' + \gamma\alpha') E_{xz} \\
&\quad + (\beta\gamma' + \gamma\beta') E_{yz}.
\end{aligned} \tag{A3}$$

The Slater-Koster matrix elements  $V_{pp\sigma}$  and  $V_{pp\pi}$  are given by equ.(3) and contain the distance dependence.

- 
- [1] D.D.Eley and D.I.Splivey, Trans. Faraday Soc., **58**, 411 (1962)
  - [2] M.A.Young, G.Ravishanker and D.L.Beveridge, Biophys.J., **73**, 2313 (1997)
  - [3] P.J.de Pablo *et al*, Phys.Rev.Lett. **85**, 4992 (2000)
  - [4] D.Porath, A.Bezryadin, S. De Vries, and C.Decker, Nature (London) **403**, 635 (2000)
  - [5] H.W. Fink and C. Schönenberger, Nature **398**, 407 (1999).
  - [6] A.Y.Kasumov *et al*, Science **291**, 280 (2001)
  - [7] L.Cai, H.Tabata, and T.Kawai, Appl.Phys.Lett. **77**, 3105 (2000)
  - [8] D.Sánchez-Portal, P.Ordejón, E.Artacho, and J.M.Soler, Int.J.Quantum Chem. **65**, 453 (1997);  
E.Artacho, D.Sánchez-Portal, P.Ordejón, A.Garcia, and J.M.Soler, Phys.Status Solidi (b) **215**,  
809 (1999); P.Ordejón, E.Artacho, J.M.Soler, Phys.Rev.B **53**, R10441 (1996)
  - [9] C.Wan, T.Fiebrig, O.Schiemann, J.K.Barton, A.H.Zewail, PNAS **97**, 14052
  - [10] R.Chandrasekaran and S.Arnott, J.Biomol.Struct. Dynamics, **13**, 1015 (1996)
  - [11] S.Arnott and D.W.L.Hukins, Biochem.Biophys.Res.Comm., **47**, 1504 (1972)

- [12] D.Bensimon, A.J.Simon, V.Croquette, A.Bensimon, *Phys.Rev.Lett.* **74**, 4754 (1995); J.F.Allemand *et al*, *Biophys.J.*, **73**, 2064 (1997); I.Parra and B.Windle, *Nature Genetics*, **5**, 17 (1993)
- [13] A.Lebrun and R.Lavery, *Nucl.Acids Res.*, **24**, 2260 (1996); M.W.Konrad and J.I.Bolonick, *J.Am.Chem.Soc.*, **118**, 10989 (1996); K.M.Kosikov *et al*, *J.Mol.Biol.*, **289**, 1301 (1999)
- [14] M.D.Newton, *J.Phys.Chem.*, **90**, 3734 (1986)
- [15] H.Sugiyama and I.Saito, *J.Am.Chem.Soc.* **118**, 7063 (1996); M.L.Zhang, M.S.Miao, V.E. van Doren, J.J. Ladik, J.W.J.Mintmire, *J.Chem.Phys.* **111**, 8696 (1999)
- [16] W.A.Harrison, *Electronic Structure and the Properties of Solids*, Dover Publications, Inc., New York, p.48,481 (1989)
- [17] M.A.Young, B.Jayaram, and D.L.Beveridge, *J.Am.Chem.Soc.* **119**, 59 (1997); A.P.Lyubartsev, A.Laaksonen, *J.Biomol.Struct.Dynamics* **16**, 579 (1998); Alexandre M.J.J. Bonvin, *Eur.Biophys.J.* **29**, 57 (2000)
- [18] S.Priyadarshy, S.M.Risser and D.N. Beratan, *J.Phys.Chem.* **100**, 17678 (1996)
- [19] R.A.Marcus and N.Sutin, *Biochim.Biophys.Acta* **811**, 265 (1985)
- [20] L.D.Landau, *Phys.Z. Sowjetunion* **1**, 88 (1932); **2** 46 (1933); C.Zener, *Proc.R.Soc. London A* **137**, 696 (1932); **140** 660 (1933)
- [21] A.Klimk̄ans and S.Larsson, *Chem.Phys.* **189**, 25 (1994)
- [22] C.T.Chan, K.M.Ho and W.A.Kamitakahara, *Phys.Rev.B* **36**, 3499 (1987)
- [23] A.Harriman, *Angew.Chem.Int.Ed.Engl.* **38**, 945 (1999)
- [24] M.Bixon and J.Jortner, *J.Am.Chem.Soc.* **123**, 12556 (2001)
- [25] S.Steenken and S.V.Jovanovic, *J.Am.Chem.Soc.* **119**, 617 (1997); C.A.M.Seidel, A.Schulz and M.H.M.Sauer, *J.Phys.Chem.* **100**, 5541 (1996)
- [26] J.Jortner, M.Bixon, T.Langenhacher and M.E.Michel-Beyerle, *Proc.Natl.Acad.Sci. U.S.A* **95**, 12759 (1998)
- [27] F.D.Lewis *et al*, *Science* **277**, 673 (1997)



TABLE I: Transfer integrals in eV between HOMOs ( $t_H$ ) and LUMOs ( $t_L$ ) of two base pairs. The calculations are done with SIESTA and DZP basis set.

	A DNA		B DNA	
dimer	$t_H$	$t_L$	$t_H$	$t_L$
GG	0.0069	-0.0006	-0.1409	0.0525
GG(2.425Å) <sup>a</sup>			-0.6922	0.2548
GG(0.0°) <sup>b</sup>			0.2385	0.3233
5'-AG-3'	-0.0153	0.0060	-0.0710	0.1124
5'-GA-3'	-0.0113	-0.0010	-0.1871	0.0472
AA	0.0310	-0.0120	-0.0695	0.1054
Ribbon				
GG	0.0039	0.0083		

<sup>a</sup>corresponds to perpendicular base pair separation of A DNA which has a tilt angle of 20°. Note the huge difference to A form GG.

<sup>b</sup>perfectly parallel aligned base pairs. Note the sign change compared to B form GG at 36°.

TABLE II: Inner reorganization energies  $E_{\lambda,i}$ , moments of inertia  $I$  and nuclear frequencies  $\nu_n$  of single base pairs. The calculations are done with SIESTA and DZP basis set.  $E_{\lambda,i}$  is determined by the energy difference of a hole/electron doped base pair between doped and undoped relaxed geometries. The moment of inertia is estimated with  $I = \sum m_i r_i^2$  where the sum is over all atoms of a base pair and  $r_i$  are measured from the helical axis of B DNA. The nuclear frequencies are derived with  $E_{\lambda,i} = 2(\pi\nu)^2 \sum \mu_{i,i+1} u_{i,i+1}^2$  with  $\mu_{i,i+1}$  and  $u_{i,i+1}$  being the reduced mass and change in bond length of atoms  $i$  and neighbor  $i+1$  when comparing doped with undoped relaxed structures.

		G·C	A·T
$E_{\lambda,i}$ [eV]	hole	0.18	0.08
	electron	0.28	0.20
$I$ [10 <sup>-44</sup> kg m <sup>2</sup> ]		5.0	6.2
$\nu_n$ [10 <sup>13</sup> 1/s]	hole	3.97	3.64
	electron	5.09	2.74

TABLE III: Oscillation time of twisting motion  $T_S$ , total reorganization energy  $E_\lambda \approx \sum E_{\lambda,i}$ , Franck-Condon factor FC, and upper/lower limits of adiabatic charge transfer rates between two neighboring base pairs (bps). The rates are calculated with equ.(12) and data from table (II) in the normal regime. The upper limit corresponds to a nuclear frequency  $1/\nu = 1/\nu_n^1 + 1/\nu_n^2$ , the lower limit to  $\nu = 1/T_S$ .

sequence <sup>a</sup>		GG	AG <sup>b</sup>	AA
$T_S$ [ps]		2.02	2.13	2.25
$E_\lambda$ [eV]	hole	0.36	0.26	0.16
	electron	0.57	0.48	0.39
FC (at 300K)	hole	0.03	0.88	0.22
	electron	0.004	0.01	0.02
	limit			
$k_{hole}$ [1/s]	upper	$6.0 \cdot 10^{11}$	$1.7 \cdot 10^{13}$	$4.1 \cdot 10^{12}$
	lower	$1.5 \cdot 10^{10}$	$4.1 \cdot 10^{11}$	$9.9 \cdot 10^{10}$
$k_{electron}$ [1/s]	upper	$1.1 \cdot 10^{11}$	$1.8 \cdot 10^{11}$	$3.1 \cdot 10^{11}$
	lower	$2.1 \cdot 10^9$	$4.7 \cdot 10^9$	$1.0 \cdot 10^{10}$

<sup>a</sup>electron transfer actually involves the complementary basis C and T.

<sup>b</sup>we used the following reaction energies: hole transfer between A and G,  $E_o = -0.2$  eV; electron transfer between T and C,  $E_o \approx 0$  eV.

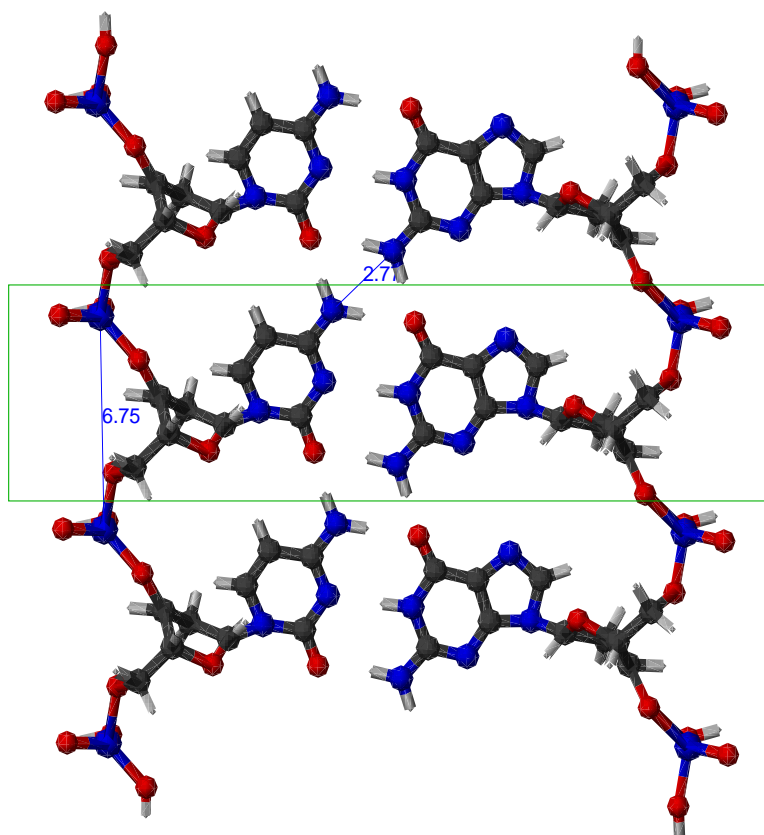


FIG. 1: Ideal 2-dimensional ribbon structure for DNA stretched by factor 2. The green box indicates the unit cell of height  $6.75\text{\AA}$ . There are only very few good contacts.

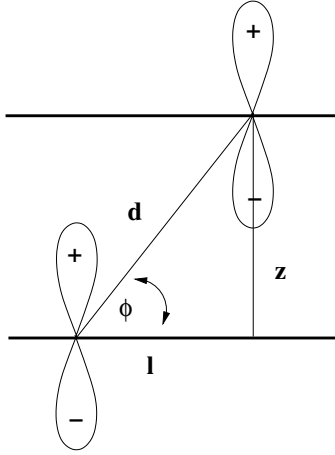


FIG. 2: Interatomic matrix elements from Slater-Koster theory: two atomic  $p_z$  orbitals on adjacent base pairs couple by positive  $pp\sigma$  and negative  $pp\pi$  interactions.

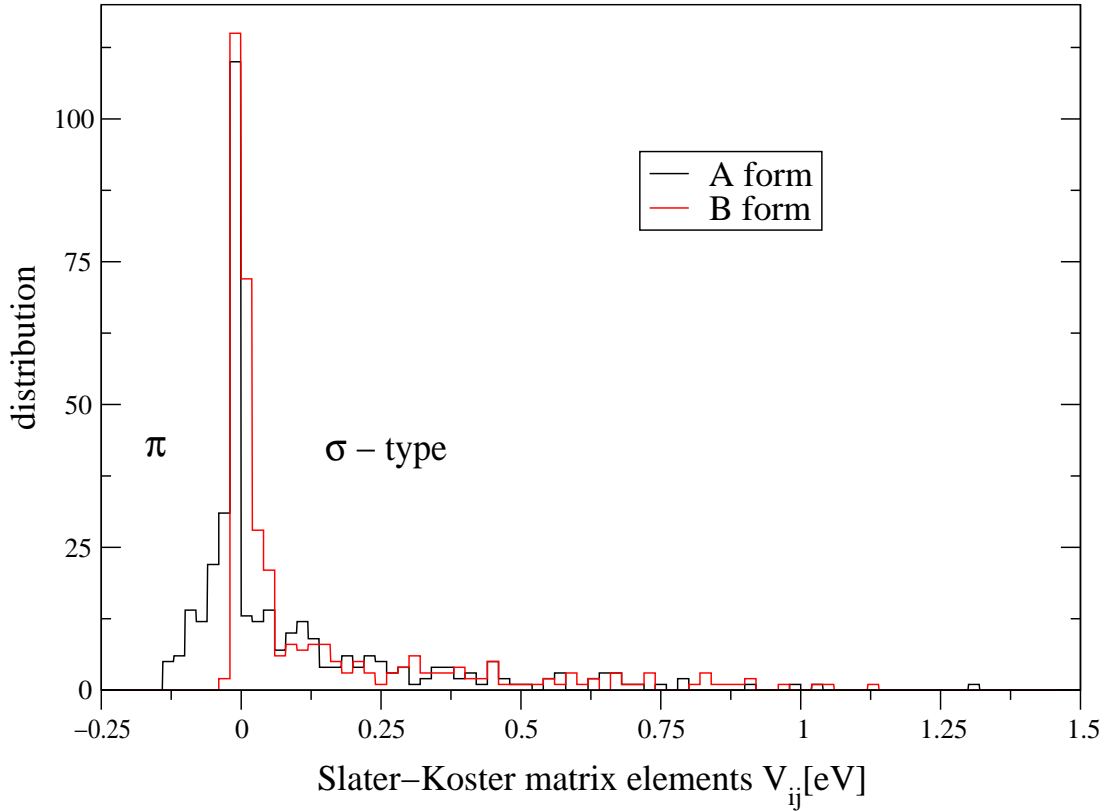


FIG. 3: Distribution of Slater-Koster interatomic matrix elements between  $p_z$  orbitals of two stacked  $G \cdot C$  base pairs. There is a total of 361 matrix elements. The smallest peak height corresponds to a single matrix element. Details about the distributions, mean: A 0.09, B 0.13; standard deviation: A 0.21, B 0.23; number of matrix elements above 0.75eV: A 6, B 13.

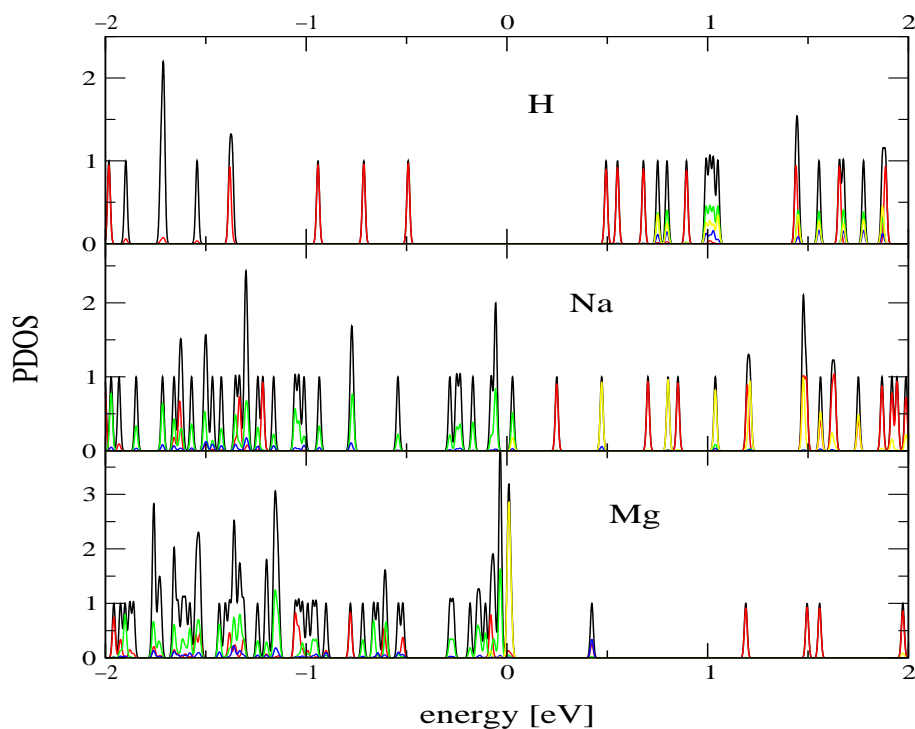


FIG. 4: Effects of different counterions on the molecular orbitals of B DNA; black: total DOS, red:  $p_z$  orbitals within base pairs, green: phosphate, blue: sugar, yellow: counterions. The Fermi energy is set to 0 eV.

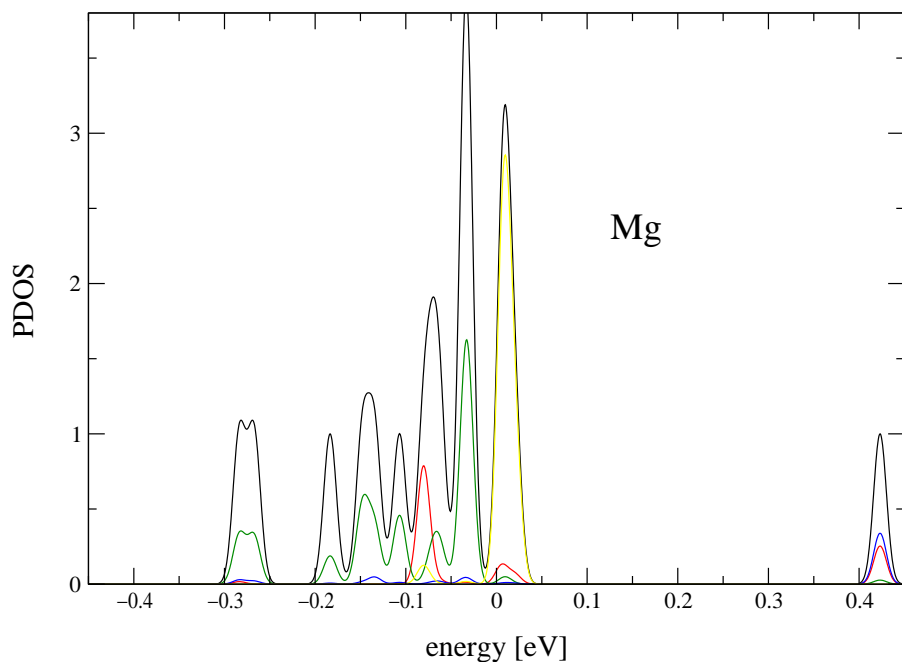


FIG. 5: Can magnesium ions make DNA conducting? Blow up of the PDOS near the Fermi energy; black: total DOS, red:  $p_z$  orbitals within base pairs, green: phosphate, blue: sugar, yellow: magnesium.

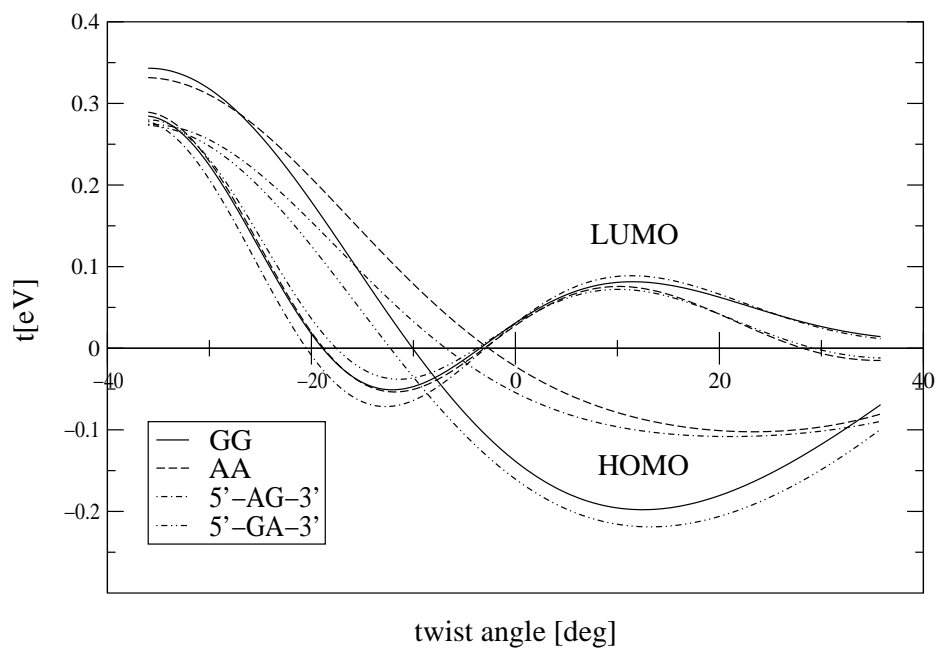


FIG. 6: Change of electronic coupling between frontier orbitals of two base pairs with relative twist angle  $\phi$  about the equilibrium position. The base pair separation is kept fixed at  $z = 3.375 \text{ \AA}$ .

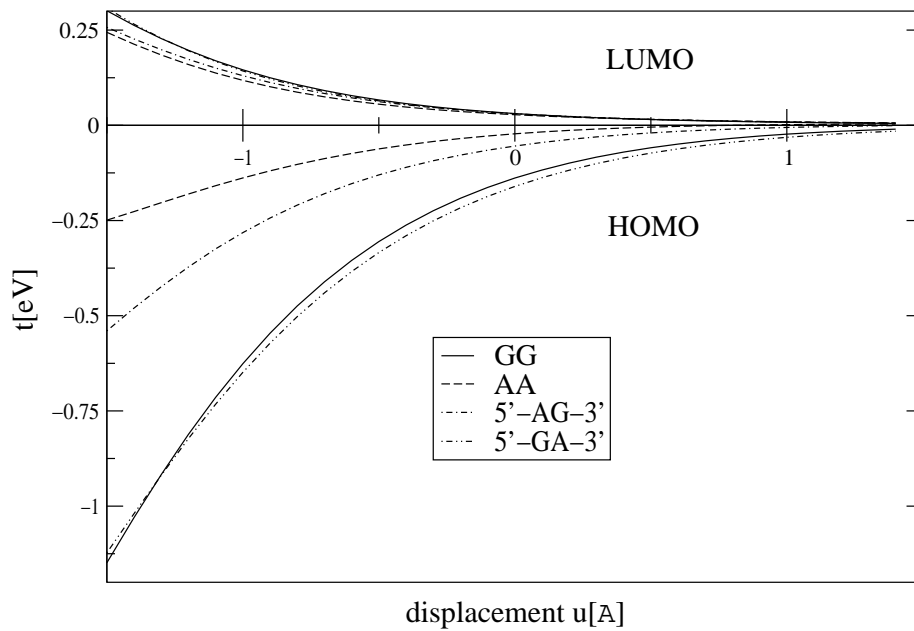


FIG. 7: Change of electronic coupling with relative displacement  $u$  about the equilibrium position. The twist angle is kept fixed at  $36.0^\circ$ .

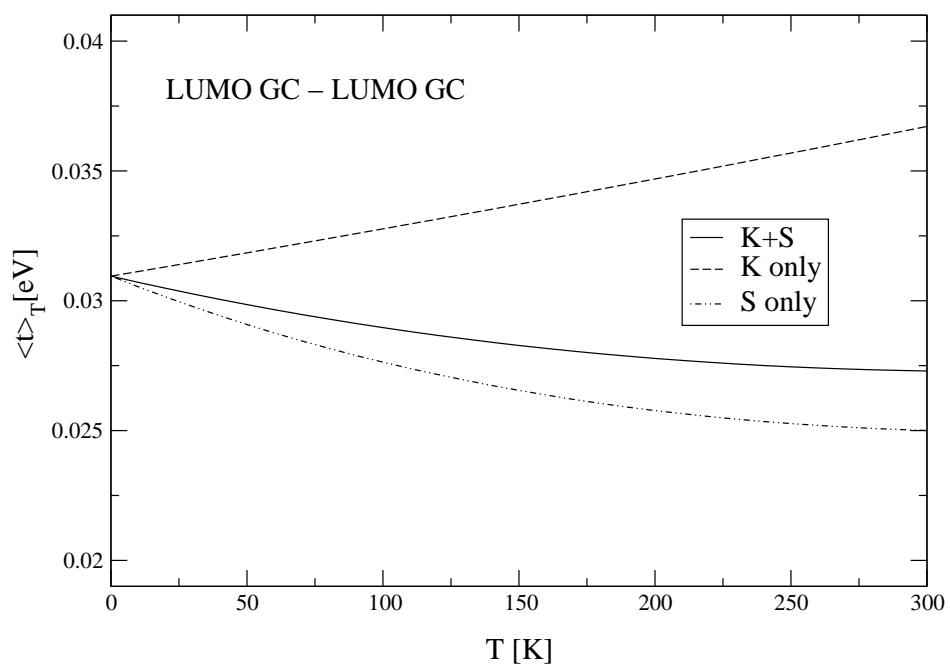


FIG. 8: Boltzmann averaged electronic coupling between LUMOs of two  $G \cdot C$  base pairs as a function of temperature  $T$ . The effects of a spring constant  $K$  and a shear constant  $S$  are shown.

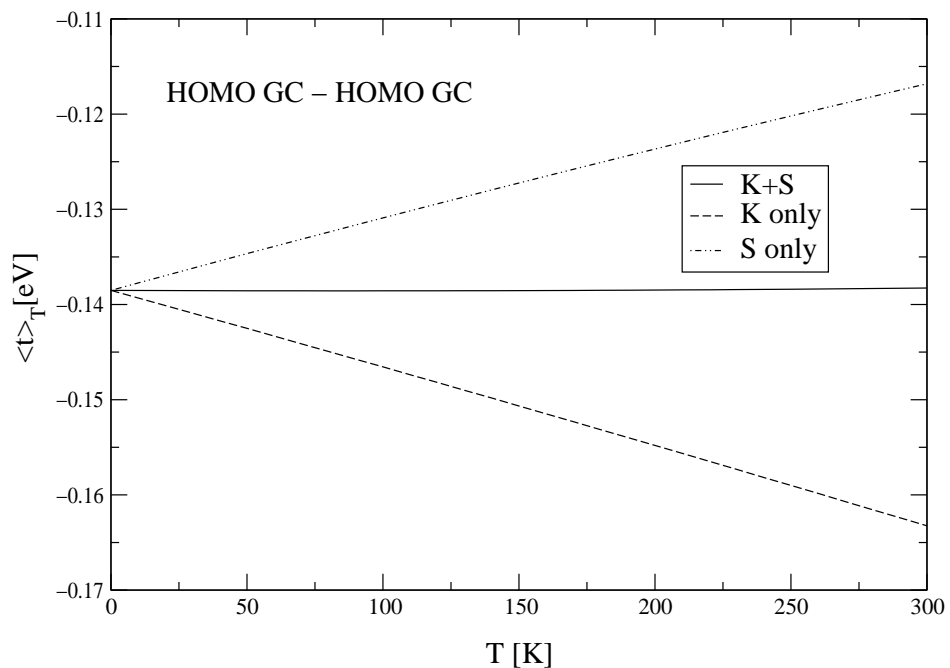


FIG. 9: Boltzmann averaged electronic coupling between HOMOs of two  $G \cdot C$  base pairs as a function of temperature  $T$ . The effects of a spring constant  $K$  and a shear constant  $S$  are shown.